Sheffield Hallam University

The shear viscosity of a two-dimensional emulsion of drops using a multiple-relaxation-time-step lattice Boltzmann method

HALLIDAY, Ian <http://orcid.org/0000-0003-1840-6132>, XU, Xu <http://orcid.org/0000-0002-9721-9054> and BURGIN, Kallum

Available from Sheffield Hallam University Research Archive (SHURA) at:

https://shura.shu.ac.uk/14337/

Citation:

Shear viscosity of a two-dimensional emulsion of drops using a multiple-relaxation-time-step lattice Boltzmann method

I. Halliday,[1,*] X. Xu,[1,2] and K. Burgin[1]

[1]*Materials & Engineering Research Institute, Sheffield Hallam University, Howard Street, Sheffield S1 1WB, United Kingdom*
[2]*Department of Engineering and Mathematics, Sheffield Hallam University, Howard Street, Sheffield S1 1WB, United Kingdom*

An extended Benzi-Dellar lattice Boltzmann equation scheme [R. Benzi, S. Succi, and M. Vergassola, Europhys. Lett. **13**, 727 (1990); Phys. Rep. **222**, 145 (1992); P. J. Dellar, Phys. Rev. E **65**, 036309 (2002)] is developed and applied to the problem of confirming, at low Re and drop fluid concentration, c, the variation of effective shear viscosity, $\eta_{\text{eff}} = \eta_1[1 + f(\eta_1,\eta_2)c]$, with respect to c for a sheared, two-dimensional, initially crystalline emulsion [here η_1 (η_2) is the fluid (drop fluid) shear viscosity]. Data obtained with our enhanced multicomponent lattice Boltzmann method, using average shear stress and hydrodynamic dissipation, agree well once appropriate corrections to Landau's volume average shear stress [L. Landau and E. M. Lifshitz, *Fluid Mechanics*, 6th ed. (Pergamon, London, 1966)] are applied. Simulation results also confirm the expected form for $f(\eta_i,\eta_2)$, and they provide a reasonable estimate of its parameters. Most significantly, perhaps, the generality of our data supports the validity of Taylor's disputed simplification [G. I. Taylor, Proc. R. Soc. London, Ser. A **138**, 133 (1932)] to reduce the effect of one hydrodynamic boundary condition (on the continuity of the normal contraction of stress) to an assumption that interfacial tension is sufficiently strong to maintain a spherical drop shape.

I. INTRODUCTION

Since the work of Gunstensen and Rothman [1], several multicomponent lattice Boltzmann equation (MCLB) methods have been developed. Broadly, a variant may be classified by the physical content of its fluid-fluid interface algorithm. Where the kinematics of phase separation must be considered, *free-energy* methods [2,3] and their thermodynamically consistent extensions, due to Wagner and co-workers [4–6], based, as they are, on the Cahn-Hilliard theory, are appropriate. For workers with a background in molecular simulation, the Shan-Chen method [7] is a natural choice. In this work, we consider the MCLB interface of Lishchuk *et al.* [8], which is adapted to completely arrested coalescence, i.e., to completely immiscible fluids, considered in the continuum approximation. Used with appropriate component segregation [9], this method furnishes a robust technique with interfacial tension effects that conform with Laplace's law and continuum interfacial kinematics and dynamics. A further advantage is that one can restrict computational memory requirements, such that, in two dimensions, for a number of immiscible components $M > 5$, computational memory requirements barely increase and execution times increase only slowly [10–12].

All MCLB models contain an interfacial microcurrent, spurious velocity, or parasitic current, induced in the immediate vicinity of the fluid-fluid interface. This unphysical artefact restricts the applicability of MCLB, particularly to the continuum regime, where the capillary number (Ca) is small. This is unfortunate since the lattice Boltzmann simulation is otherwise an attractive tool for such applications. Lee and Fischer [13] and Pooley and Furtado [14] have successfully addressed the elimination of spurious flow from free-energy-type

MCLBs in the past. Their approaches do not, however, generalize to Lishchuk's continuum method.

The effect of the microcurrent may be very important in continuum applications. Clearly any error it introduces will be most restrictive when Re and Ca are both small: as one departs from this regime, the effect of the microcurrent will diminish. It is important, therefore, to assess Lishchuk's method in this regime, and the most apparent test is to attempt to measure the effective viscosity, η_{eff}, of a monodisperse emulsion of immiscible drops of one liquid suspended in another, at low Re and concentration c, for here analytical predictions may be used to assess data. In this work, we choose to treat what is initially a two-dimensional crystal of immiscible drops of neutrally buoyant liquid of viscosity η_2 suspended (at low concentration) within a sheared liquid of viscosity η_1. It would be very valuable indeed to be able to observe the linear regime of the response in which $\eta_{\text{eff}} = [1 + f(\eta_1,\eta_2)c]$, for such data would support the conclusion that a microcurrent is not a great limitation on the appropriate application of MCLB, even to the low Re Stokes regime.

In Sec. II, we review Lishchuk's MCLB. Since it is known that a viscosity contrast creates simulation noise, it is necessary to develop a multirelaxation time variant of the Lishchuk method, and an extended method based upon the model of Benzi *et al.* [15,16] and Dellar's shallow water LB scheme [17] is developed in Appendix A. This model is then applied to the problem of computing the viscosity of emulsions, as described in Sec. III. We then present our results in Sec. IV and our conclusions in Sec. V.

II. BACKGROUND

In Lishchuk's MCLB method, Laplace law and "no-traction" effects (i.e., the continuity of the tangential contraction of stress [18]) arise from a curvature-dependent external

---

*Author to whom all correspondence should be addressed: i.halliday@shu.ac.uk

023301-1

force density, impressed primarily in regions where the fluid components' phase field varies most rapidly. Let two fluid distributions occupying lattice link i at position $\mathbf{x}$ be described by distribution functions, $R_i(\mathbf{x})$ and $B_i(\mathbf{x})$ [of course with $f_i(\mathbf{x}) = R_i(\mathbf{x}) + B_i(\mathbf{x})$]. The nodal density of the red and blue fluids,

$$\rho_R(\mathbf{x}) = \sum_i R_i(\mathbf{x}), \quad \rho_B(\mathbf{x}) = \sum_i B_i(\mathbf{x}), \qquad (1)$$

is used to define a local phase field [9]:

$$\rho^N(\mathbf{x}) = \frac{\rho_R(\mathbf{x}) - \rho_B(\mathbf{x})}{\rho_R(\mathbf{x}) + \rho_B(\mathbf{x})}. \qquad (2)$$

Surfaces $\rho^N = \text{const}$ define the interface, with $\rho^N = 0$ its center. Throughout the narrow but finite and distributed interfacial region, the local interface normal is obtained from numerical approximations for the following:

$$\hat{\mathbf{n}} = -\frac{\boldsymbol{\nabla}\rho^N}{|\boldsymbol{\nabla}\rho^N|}. \qquad (3)$$

With the above definition, for a red drop in a blue fluid, the interface normal unit vector $\hat{\mathbf{n}}$ points away from the enclosed red fluid. Local interfacial curvature is obtained from the surface gradient of $\hat{\mathbf{n}} = (\hat{n}_x, \hat{n}_y)$, which, in two dimensions, is given by [8]

$$\kappa \equiv \hat{n}_x \hat{n}_y \left(\frac{\partial \hat{n}_y}{\partial x} + \frac{\partial \hat{n}_x}{\partial y} \right) - \hat{n}_y^2 \frac{\partial \hat{n}_x}{\partial x} - \hat{n}_x^2 \frac{\partial \hat{n}_y}{\partial y}. \qquad (4)$$

All the derivatives in Eqs. (3) and (4) are usually computed to $o(\mathbf{c}_i^4)$ accuracy with a simple, local, compact stencil:

$$\frac{\partial f}{\partial x_\alpha} = \frac{1}{k_2} \sum_{i \neq 0} t_i f(\mathbf{x} + \mathbf{c}_i) c_{i\alpha} + o(\mathbf{c}_i^4), \quad x_\alpha \in [x, y], \qquad (5)$$

where the lattice isotropy constant $k_2 = c_s^2 = 1/3$ for the D2Q9 lattice used in this work. Clearly, the number of grid points required to calculate a gradient depends upon the cardinality of the LBE lattice unit cell's basis set, Q. Interfacial tension effects arise when the following normally directed Lishchuk force density is applied:

$$\mathbf{F} = \tfrac{1}{2}\sigma\kappa\boldsymbol{\nabla}\rho^N, \qquad (6)$$

in which σ is an interfacial tension parameter and κ is the interface curvature. In Eq. (6), factor $\frac{1}{2}\boldsymbol{\nabla}\rho^N$ acts as a weight [8]. The force distribution in Eq. (6) may be shown to recover correct dynamics for the continuum regime [8]. That is, a Laplace law pressure step [19] across interfacial regions (given by $\sigma\kappa$ in two dimensions) and the no-traction condition arise from the force density in Eq. (6). Correct interfacial motion kinematics arise from an appropriate segregation step, and the kinematic property of mutual impenetrability emerges from correctly chosen, postcollision color segregation rules [20], developed from the work of D'Ortona *et al.* [21].

The Lishchuk force is applied as an external force density to what is effectively a single fluid, described by the distribution function $f_i = R_i + B_i$. The latter is evolved using a multiple-relaxation-time-scheme method presented in Appendix A, where we extend the particularly suitable variant of Benzi *et al.* [15,16] and Dellar [17] to accommodate the necessary spatially variable body force, such as the Lishchuk force

in Eq. (6). Our technique after Benzi and Dellar is based upon the modified evolution of a set of carefully selected macroscopic modes (note that not all of the modes are physical). For the LB variant derived in Appendix A, the lattice fluid kinematic viscosity is set by the chosen value of one particular degenerate eigenvalue of the collision matrix, or the stress-mode relaxation parameter, designated λ_3:

$$\nu = \frac{1}{6}\left(\frac{2}{\lambda_3} - 1\right) \iff \lambda_3 = \frac{1}{6\nu + 1} \qquad (7)$$

in lattice units. See Appendix A. To introduce a viscosity contrast between the red drop fluid (shear viscosity η_2) and the blue external fluid (shear viscosity η_1), a viscosity field may be defined in terms of the phase field ρ^N as follows:

$$\nu \equiv \frac{\eta}{\rho} = \frac{1}{2}(1 - \rho^N)\nu_1 + \frac{1}{2}(1 + \rho^N)\nu_2, \qquad (8)$$

with the variable value of λ_3 determined using Eqs. (7) and (8). Note that since the kinematic viscosity is set by the value of λ_3, care must be exercised in evaluating the viscosity contrast parameter:

$$\Lambda \equiv \frac{\eta_2}{\eta_1} = \frac{\nu_2\rho_2}{\nu_1\rho_1}, \qquad (9)$$

since the interior pressure $c_s^2\rho_2$ will differ from the external pressure $c_s^2\rho_1$ by the Laplace pressure $\sigma\kappa$. Here η_1 (η_2) is the exterior (interior) fluid shear viscosity. No confusion should arise between the scalar viscosity ratio defined above and the matrix of eigenvalues, Λ, which appears only in the Appendixes.

III. METHOD

Unless otherwise stated, we use the notation of Landau and Lifshitz [19] throughout this section. At low Reynolds number, an effective viscosity for a low volume fraction sheared emulsion of spherical liquid drops, i.e., viscosity η_2, in an immiscible fluid of shear viscosity η_1 may be defined in terms of a measurement of volume-averaged viscous dissipation, $\overline{D}$, as follows [22]:

$$\eta_{\text{eff}} = \eta_1[1 + \phi(\eta_1, \eta_2)c] = \frac{\overline{D}}{\dot{\gamma}^2}. \qquad (10)$$

Here c is the concentration, $\dot{\gamma} = \overline{\frac{\partial v_x}{\partial y}}$ is the volume-averaged shear rate, and for a complex fluid with spatially variable composition,

$$\overline{D} = -\frac{1}{2V} \int \eta \sigma'_{ij} \sigma'_{ij} dV. \qquad (11)$$

Landau and Lifshitz, using the fact that the effective viscosity must also control the mean transport of horizontal momentum in the vertical direction, obtain another expression based upon a volume average of viscous stress component σ'_{ij} [19]. We show in the Appendixes that their analysis requires minor modification when applied to MCLB, where body forces, $\mathbf{F}$, are present:

$$\eta_{\text{eff}} = \frac{\overline{\sigma'_{xy}} - \int y F_x dV}{\dot{\gamma}}, \qquad (12)$$

where

$$\overline{\sigma'_{xy}} = \frac{1}{V} \int \sigma'_{xy} \, dV. \tag{13}$$

Note that the volume integrals in Eqs. (11)–(13) are computed as lattice summations, with the appropriate MCLB viscous stress as given in Eq. (A27) of Appendix A. We expect the data for η_{eff} based upon Eqs. (10) and (12) to be consistent.

The correction term that appears in Eq. (12) is expected to be small. For the case of a well-resolved, negligibly deformed (circular) drop centered exactly on the origin, we expect $F_x(x, y) = -F_x(-x, y)$. However, in finite simulations it will be shown (in Sec. IV) to affect the results significantly.

A single drop of constant radius $R = 20$ lattice units was placed at the center of a square lattice, side length L, and a shear was applied using a Lees-Edwards boundary condition [23,24] for which the shear parameter was set to maintain a small, constant Reynolds number:

$$\text{Re} = \frac{\dot{\gamma} L^2 \rho}{\nu} = 0.01. \tag{14}$$

Note that our use of the Lees-Edwards boundary condition of Wagner *et al.* and Lorentz *et al.* allows a single drop to interact with an array of periodic replicas effectively to produce a crystalline emulsion of cylindrical drops, the spacings of which vary with time and the concentration of which is

$$c = \frac{\pi R^2}{L^2} \leqslant 0.05. \tag{15}$$

The value of c was varied by adjusting L with the appropriate Lees-Edwards parameter determined from Eq. (14).

In Sec. IV we shall infer from data, subject to the above considerations, the functional form of the shear viscosity of a two-dimensional emulsion of neutrally buoyant cylindrical drops, shear viscosity η_2, within a liquid of shear viscosity η_1. It will be necessary to consider a wide range of shear viscosity contrast, Λ, which necessitates the improvement in stability afforded by a multiple-relaxation-time-step (MRT) lattice Boltzmann equation method (LBE). Moreover, the need to apply an immersed boundary-type force effect (to produce interfacial tension) means that our "forced" MRT LBE must carry a spatially variable fluid body-force density. The particular D2Q9 method we develop for this purpose is based on Dellar's [17] because, in its original form (without a body force), it is efficient (due to its use of nonhydrodynamic modes N, J_x, and J_y [17] with zero equilibria), robust, and straightforward to implement. Our extended form is expressed by the following kinetic evolution equation:

$$f_i(\mathbf{x} + \mathbf{c_i}\delta t, t + \delta t) = f_i(\mathbf{x}, t) + \sum_j A_{ij} \left[f_j^{(0)}(\mathbf{x}, t) - f_j(\mathbf{x}, t) \right] + \delta t \, F_i, \tag{16}$$

where

$$f_j^{(0)} = \rho t_j \left(1 + 3 u_\alpha c_{j\alpha} + \tfrac{9}{2} u_\alpha u_\beta c_{j\alpha} c_{j\beta} - \tfrac{3}{2} u_\gamma u_\gamma \right). \tag{17}$$

Here, the source term F_i has the following properties:

$$\sum_i F_i = 0, \quad \sum_i \mathbf{c}_i F_i = n\mathbf{F}, \quad \sum_i \mathbf{c}_i \mathbf{c}_i F_i = \frac{1}{2}[\mathbf{C} + \mathbf{C}^T], \tag{18}$$

while the eigenspectrum of the collision matrix A_{ij} (identified in Table I) supports the following:

$$\sum_i 1_i A_{ij} = 0, \quad \sum_i c_{i\alpha} A_{ij} = 0, \quad \sum_i c_{i\alpha} c_{i\beta} A_{ij} = \lambda_3 c_{j\alpha} c_{j\beta}. \tag{19}$$

Here α and β represent x or y. Weighting factors, t_i, and the lattice isotropy properties defined in terms of them (see Hou *et al.* [25]) take the usual form, explicitly stated in Appendix A.

Now, the collision matrix A_{ij} is defined by nine linearly independent left-row eigenvectors, $\mathbf{h}^{(p)}$, $p = 0, \dots, 8$, and their eigenvalues λ_p. Three eigenvectors that are the projectors of the hydrodynamic modes of ρ and $\rho\mathbf{v}$ must have $\lambda_0 = \lambda_1 = \lambda_2 = 0$, and another three, which essentially project components of two-dimensional (2D) stress $P_{\alpha\beta}$, must be degenerate: $\lambda_3 = \lambda_4 = \lambda_5$. We follow Benzi *et al.* [15,16] and Dellar [17] in selecting the three remaining "ghost" eigenvectors N, J_x, and J_y with eigenvalues λ_6 and $\lambda_7 = \lambda_8$. The complete set of $\mathbf{h}^{(p)}$'s in Table I define a matrix of left-row eigenvectors $\mathbf{M} \equiv (\mathbf{h}^{(0)}, \mathbf{h}^{(1)}, \dots, \mathbf{h}^{(8)})^T$, which is the projector of all nine modes:

$$(\rho, \rho u_x, \rho u_y, P_{xx}, P_{yy}, P_{xy}, N, J_x, J_y)^T = \mathbf{M} \mathbf{f}, \quad \mathbf{f} \equiv (f_0, f_1, f_2, \dots, f_8)^T. \tag{20}$$

TABLE I. Eigenvalues, left-row eigenvectors, and equilibria of the collision matrix, where $i = 0, \dots, 8$.

Mode	Component	Definition	Eigenvalue	Projection	Physical interpretation	Equilibrium
$\mathbf{h}^{(0)}$	$h_i^{(0)}$	1	0	ρ	density	ρ
$\mathbf{h}^{(1)}$	$h_i^{(1)}$	c_{ix}	0	ρu_x	x momentum	ρu_x
$\mathbf{h}^{(2)}$	$h_i^{(2)}$	c_{iy}	0	ρu_y	y momentum	ρu_y
$\mathbf{h}^{(3)}$	$h_i^{(3)}$	c_{ix}^2	λ_3	P_{xx}	xx viscous stress	$\Pi_{xx}^{(0)}$
$\mathbf{h}^{(4)}$	$h_i^{(4)}$	c_{iy}^2	λ_3	P_{yy}	yy viscous stress	$\Pi_{yy}^{(0)}$
$\mathbf{h}^{(5)}$	$h_i^{(5)}$	$c_{ix} c_{iy}$	λ_3	P_{xy}	xy viscous stress	$\Pi_{xy}^{(0)}$
$\mathbf{h}^{(6)}$	$h_i^{(6)}$	g_i	λ_6	N		0
$\mathbf{h}^{(7)}$	$h_i^{(7)}$	$g_i c_{ix}$	λ_7	J_x		0
$\mathbf{h}^{(8)}$	$h_i^{(8)}$	$g_i c_{iy}$	λ_7	J_y		0

Using **M**, Eq. (16) may be projected as

$$\mathbf{M}\,\mathbf{f}^+ = \mathbf{M}\,\mathbf{f} + \mathbf{M}\,\mathbf{A}\,\mathbf{M}^{-1}(\mathbf{M}\,\mathbf{f}^{(0)} - \mathbf{M}\,\mathbf{f}) + \mathbf{M}\,\mathbf{F}, \quad (21)$$

where **F** denotes the column vector with elements F_i; **f**, **f**$^+$, and **f**$^{(0)}$ are also column vectors. Since the **h**$^{(\mathbf{n})}$ are left-row eigenvectors of **A**, it follows that $\mathbf{M}\,\mathbf{A} = \Lambda\,\mathbf{M} \Leftrightarrow \Lambda = \mathbf{M}\,\mathbf{A}\,\mathbf{M}^{-1}$, with Λ the diagonal matrix $\Lambda = \mathrm{diag}(\lambda_0, \lambda_1, \ldots, \lambda_8)$. Clearly, therefore, Eq. (16) may be written in component form:

$$h^{(p)+} = h^{(p)} + \lambda_p(h^{(0)(p)} - h^{(p)}) + S^{(p)}, \quad (22)$$

$$S^{(p)} = \sum_{j=0}^{8} M_{pj} F_j, \quad p \in [0, Q]. \quad (23)$$

Expressions for all nine modal source terms, $S^{(p)}$, and equilibria, $h^{(0)(p)}$, are derived in Appendix A, where we show that it is possible to invert **M** and to reconstruct a postcollision distribution function vector **f**$^+$:

$$\mathbf{f}^+ = \mathbf{M}^{-1}(\rho^+, \rho u_x^+, \rho u_y^+, P_{xx}^+, P_{yy}^+, P_{xy}^+, N^+, J_x^+, J_y^+)^T, \quad (24)$$

which can be shown to yield the following expressions for the forced, postcollision distribution function:

$$
\begin{aligned}
f_i^+ &= (M)_{ij}^{-1} h_j^+ \\
&= t_i \Bigg\{ \left[2 - \frac{3}{2}\left(c_{ix}^2 + c_{iy}^2\right) \right]\rho + 3[(\rho u_x)^+ c_{ix} + (\rho u_y)^+ c_{iy}] \\
&\quad + \frac{9}{2}\left(P_{xx}^+ c_{ix}^2 + 2 P_{xy}^+ c_{ix}c_{iy} + P_{yy}^+ c_{iy}^2\right) - \frac{3}{2}\left(P_{xx}^+ + P_{yy}^+\right) \\
&\quad + \frac{1}{4}g_i N^+ + \frac{3}{8}g_i(J_x^+ c_{ix} + J_y^+ c_{iy}) \Bigg\}.
\end{aligned}
\quad (25)
$$

Full details of the derivation of our forced MRT LBE scheme and its weakly compressible hydrodynamics (using Chapman-Enskog analysis) may be found in Appendixes A–C.

IV. RESULTS AND DISCUSSION

All of the data presented in this section relate to a drop of radius 20 lattice units, with external fluid kinematic viscosity fixed at $\nu_1 = \frac{1}{3}$, variable internal viscosity $\nu_2 \in [\frac{1}{3}, \frac{4}{3}]$, and Re = 0.01. There is no density contrast (other than that associated with the Laplace pressure) in any of the data presented. The final value of the interior (exterior) lattice density was measured to be 1.999 88 (2.002 89), giving an external fluid shear viscosity $\eta_1 = 0.666\,578$. Concentration c was varied by increasing the lattice size, so the two-dimensional cylindrical drops studied have constant resolution.

Figure 1 shows the pressure, Stokes' stream function, and the stress fields of a sheared drop with $\Lambda = 2.5$. The imposed external shear flow is in the positive (negative) x direction at the top (bottom) of each panel. The kinematic condition of mutual impenetrability requires that the drop interface correspond to a streamline, and center of the interface coincides reasonably well with a stream-function contour: moreover, the drop clearly maintains a spherical shape. Disruption in the stress signal due to the interfacial microcurrent is small and significant only close to the interface, though it is noticeable in that region, with the flow at a large distance unaffected.
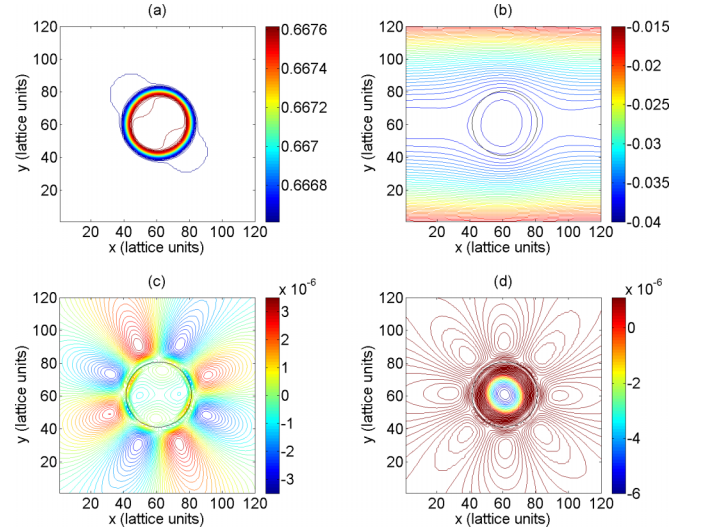

FIG. 1. Response of hydrodynamic variables to an applied shear. The external flow is to the right at the top of each panel. In (b)–(d), the central, continuous black circle indicates the phase field contour $\rho^N = 0$, which is the center of the interface. Part (a) shows isobars. Part (b) shows Stokes' stream function: note that the interface correlates reasonably with a streamline. Part (c) shows viscous stress, σ'_{xx}. Part (d) shows viscous shear stress, σ'_{xy}: the shear stress is positive throughout the external fluid, as expected.

The original effective viscosity theory of a dilute emulsion of spherical drops [22], which is based upon the calculation of the translation of a liquid sphere due independently to Rybczynski and Hadamard [26], the hydrodynamic theory of Lamb [27], and the approach of Einstein to a suspension of solid spheres [19,28], accepts *a priori* that the difficulties obstructing a complete theory are "almost insuperable." Even accepting the boundary conditions to be (a) the kinematic conditions on velocity [18] and (b) the dynamic conditions on stress contractions [19], the effects of drop distortion under shear are a formidable problem (note that the deformation of a liquid drop at low Re was later solved for simpler axisymmetric flow by Taylor and Acrivos [29]), which necessitated simplifying assumptions (of dominant interfacial tension, i.e., spherical shape and a pressure step governed by the static Laplace law) effectively to neglect the dynamic boundary condition on the normal contraction of stress, which otherwise overspecifies the solution. However, even here there is a long-standing objection to the use of a capillarity theory based upon static experiments [30], which holds that a more complicated description of interfacial stress is required, and which was shown to alter the results of Rybczynski and Hadamard [18]. Simulations of course contain chosen dynamics [which correspond here to (a) and (b) above], so that issues of numerical accuracy and dimensionality certainly notwithstanding, the data presented below are in some sense more physically complete. We reserve further comments until Sec. V.

We consider $\Lambda = 1$. The measured effective viscosity η_{eff} versus $c \in (0, 0.05]$ was computed from both Eqs. (10) and (12) independently. Reassuringly, the two resulting sets of data, shown in Fig. 2, are in excellent agreement once the stress
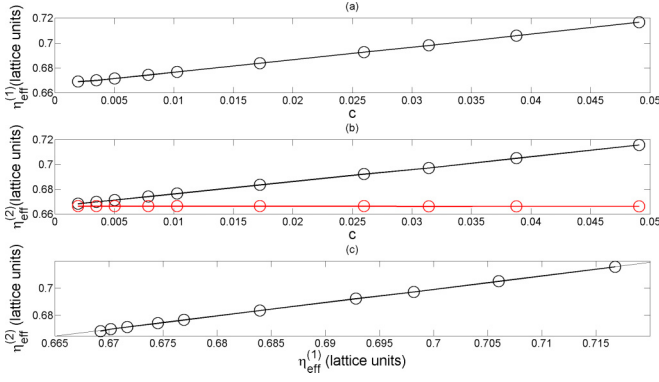
FIG. 2. Variation of emulsion effective viscosity $\eta_{\text{eff}}^{(i)}, i = 1,2$ with concentration c for $\Lambda = 1$. These data correspond to a suspension of drops that is initially octahedral. (a) $\eta_{\text{eff}}^{(1)}$ determined from measured viscous dissipation, using Eq. (10): unconstrained linear regression gives a gradient of 1.013 731 and an intercept of 0.666 657, very close to the expected value of $\eta_1 = 2/3$. (b) Black circles represent $\eta_{\text{eff}}^{(2)}$ determined from measured average shear stress, using Eq. (12), for which the gradient is 0.998 010 with an intercept of 0.666 458. The gray (red) circles represent η_{eff} derived from an average stress measurement made without applying the correction discussed in Appendix C. (c) Correlation between $\eta_{\text{eff}}^{(1)}$ and $\eta_{\text{eff}}^{(2)}$: unconstrained linear regression yields a gradient 0.9844 and an intercept 0.0102, indicating agreement between the two methods.

data are corrected as set out in Eq. (12) (we return to this point below). Without correction, the stress and dissipation data are inconsistent. The linear regression applied to both data sets is also in good agreement, and in both cases the unconstrained ordinal intercept was within 0.5% of the expected value of η_1. These data were obtained with an interfacial tension parameter $\sigma = 0.02$ lattice units. Data corresponding to a similar parametrization, with increased interfacial tensions, agree very well with that shown in Fig. 2. This observation supports the simplification made in theoretical calculations, namely to reduce the effect of one hydrodynamic boundary condition on the continuity of the normal contraction of stress to an assumption that interfacial tension is sufficiently strong to maintain a spherical drop shape.

The data presented in Fig. 2 represent one possible emulsion microstructure—that of an initial octahedral crystal of 2D drops in which identical, parallel rows of drops are moved horizontally in the applied shear, the gradient of which is vertical. While any microstructure that does not violate those assumptions made in deriving theoretical expressions for η_{eff} (again of low concentration, sufficient drop separation, low Re, and spherical shape [19,22]) must be described by Eq. (10), it is nevertheless useful to assess how a change in the microstructure of the emulsion affects the result in Fig. 2.

The data presented in Fig. 3 illustrate the effect of varying the initial emulsion microstructure. In Fig. 3, the black and red data correspond to the two different emulsion microstructures that arise when the emulsion microstructure studied in the data of Fig. 2 is varied. For the black (red) data, the vertical (horizontal) spacing of drops is fixed at 10 drop radii, and the horizontal (vertical) spacing is varied to obtain different concentrations, c. Unconstrained linear regression applied to
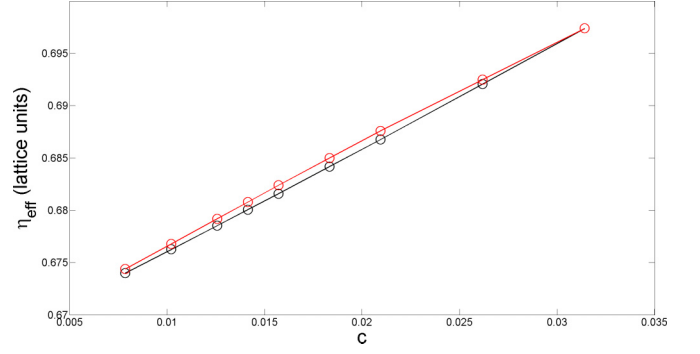

FIG. 3. The effect of emulsion microstructure on the variation of effective viscosity with concentration, for $\Lambda = 1$. The black and gray (red online) data correspond to emulsion microstructures that arise when the initial crystalline emulsion spacing is varied. For the black (gray) data, the vertical (horizontal) spacing of drops is fixed at 10 drop radii, and the horizontal (vertical) spacing is varied to obtain different concentrations, c. Unconstrained linear regression applied to the black (gray) data yields a gradient 0.9937 (0.9750) and an intercept 0.6661 (0.6669), which is in $>97\%$ agreement with the data presented in Fig. 2.

the black (red) data yields a gradient $m = 0.9937$ and an intercept $c = 0.6661$ (gradient $m = 0.9750$ and an intercept $c = 0.6669$) which is in $>97\%$ agreement with the data presented in Fig. 2. This agreement corresponds with a theory that does not allow variation of η_{eff} for any drop distribution that is sufficiently dilute. We shall henceforth take the 3% discrepancy noted between the results in Figs. 2 and 3 as an indication of our experimental error.

From Eq. (10) it follows that $\frac{d}{dc}(\frac{\eta_{\text{eff}}}{\eta_1}) = f(\eta_1,\eta_2)$. Hence, given η_1, η_2, from the gradient of a plot of the measured value of $\frac{\eta_{\text{eff}}}{\eta_1}$ versus c (similar to Fig. 2), a value of $f(\eta_1,\eta_2)$ may be calculated. On the basis of low Re three-dimensional theory [22], we expect for the two-dimensional system studied in this work

$$\phi(\eta_1,\eta_2) = \frac{\eta_1 + b\eta_2}{c\eta_1 + d\eta_2} = \frac{1 + b\Lambda}{c + d\Lambda} \equiv f(\Lambda), \qquad (26)$$

where $b, \ldots, d$ are unknown constants. Figure 4 is a plot of $f(\Lambda)$, measured in this way versus Λ. The continuous line in the top panel of Fig. 4 is an unconstrained conjugate gradients grid search that produces an optimal fit for the function of the form assumed in Eq. (26) with

$$b = 0.2393, \quad c = 0.6923, \quad d = 0.0888. \qquad (27)$$

The trend in the data in Fig. 4, which extends over two decades of parameter Λ, clearly suggests that Eq. (26) is a valid model. Moreover, at large values of Λ (made accessible by the MRT LBE scheme), Eq. (26) may be linearized:

$$\ln[f(\Lambda)] \approx m_0\Lambda^{-1} + c_0, \quad c_0 = \ln\left(\frac{b}{d}\right),$$
$$m_0 = \left(\frac{1}{b} - \frac{c}{d}\right). \qquad (28)$$

The bottom panel of Fig. 4 exhibits the linear correlation implied in Eq. (28). The value of the gradient and the intercept of a linear regression to these data—$m = -3.4741, c = 0.9862$—
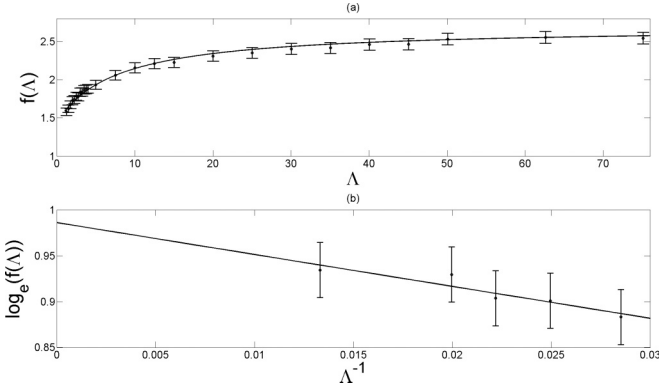
FIG. 4. (a) Gradient function $f(\Lambda)$ vs shear viscosity ratio $\Lambda = \frac{\eta_2}{\eta_1}$, where η_2 is the drop viscosity. For these data, $\eta_1 = 0.6668$ and the internal shear viscosity η_2 is adjusted following Eq. (8). The continuous line is the model function defined in Eq. (26) with optimal parameters $a = 1$, $b = 0.239$, $c = 0.692$, and $d = 0.089$. Error bars show the value of gradient $f(\Lambda)$ measured from linear regression applied to data sets such as that in Fig. 2. Bar length is determined from the error in this regression and by considering different emulsion. (b) A subset of data (for large Λ) that have been linearized, as discussed in Sec. IV. The optimal gradient and intercept are $m_0 = -3.474$ and $c_0 = 0.986$, respectively. In comparison, using the values of $a, \ldots, d$ inferred from data in the top panel, $m_0 = (\frac{1}{b} - \frac{c}{d}) = -3.614$ and $c_0 = \log_e(\frac{b}{d}) = 0.991$, which represents reasonable agreement.

are in reasonable agreement with those obtained by evaluating the expressions in Eq. (28). We note that, in contradistinction to the three-dimensional case, no theoretical expression for $\lim_{\Lambda \to \infty}[f(\Lambda)]$ exists for the data presented here.

It might be argued that the success in the linear Stokes regime of the calculations reported in this section is unsurprising. After all, in this regime the microcurrent flow stress and velocity fields (which vanish at large distance from the drop interface and are therefore compatible with most boundary conditions) are expected simply to superpose with the correct solution, which is defined by the applied boundary conditions. Thus, one might expect to obtain good data on emulsion viscosity data from appropriately corrected average stress field measurements. However, the data in Fig. 2 suggest that the effect of the microcurrent on the measured viscous dissipation (which is *not* linear in $\sigma_{\alpha\beta}$) is also restricted.

Finally, it is appropriate to state that the microcurrent generated by the interface force embedded within our MRT scheme does not differ from that produced by the single relaxation-time LBGK model [31]. Using Lishchuk's continuum method [8] in otherwise identical simulation parametrizations ($\Lambda = 1$, $R = 20$, $\sigma = 0.4$), we observe a reduction of $<10\%$ in the amplitude of the microcurrent generated by a static drop. This invariance of the microcurrent response is consistent with the current belief that the spurious field is essentially a flow response to the numerical error associated with the discretization of (for the Lishchuk method) the interface force.

V. CONCLUSIONS

Despite our comments in Sec. IV, we consider the most significant outcome from the work reported here to be that

the interfacial microcurrent does not significantly affect our low Re, two-dimensional, low-concentration effective emulsion shear viscosity data obtained with the multicomponent lattice Boltzmann simulation method, which conforms quite convincingly with the expected physical trend. This suggests that the elimination of the interfacial microcurrent is not a necessary precondition to the application of the multicomponent lattice Boltzmann method to the low Re, low-concentration regime. At higher particle concentration, however, short-range interactions must become more significant, and the influence of the interfacial microcurrent is unknown.

It is effectively Stokes' paradox that, in two dimensions, obstructs the computation of a closed-form expression for the gradient of the effective shear viscosity η_{eff} with respect to the drop fluid concentration, c, but we have obtained an empirical indication of the gradient function $f(\eta_1, \eta_2)$ in the assumed emulsion viscosity law, $\eta_{\text{eff}} = \eta_1[1 + f(\eta_1, \eta_2)]$. Data obtained with a modified lattice Boltzmann method (see below) confirm the expected form for $f(\eta_1, \eta_2)$ and provide a reasonable estimate of its parameters. Significant here is this compliance of our data (implicit in which are both dynamic stress continuity boundary conditions) with theory, which supports the validity of Taylor's theoretical simplification Ref. [22] of reducing to one hydrodynamic boundary condition (on the continuity of the normal contraction of stress) to an assumption that interfacial tension maintains a spherical drop shape. Of course, our simulation data can shed no light on the deeper, underlying disputes related to the true physical boundary conditions that apply at the drop interface Ref. [30].

Finally, the modified Benzi-Dellar lattice Boltzmann equation scheme Refs. [15–17] developed and discussed in the Appendixes works very well indeed and is essential to providing the necessary quality of data when viscosity contrasts are required in simulation.

APPENDIX A: FORCED MULTIRELAXATION-TIME LATTICE BOLTZMANN SCHEME

In this Appendix, we present a detailed derivation of the Navier-Stokes equations from the multiple-relaxation-time (MRT) lattice Boltzmann equation (LBE) where a body force is present. In the interest of a compact literature, and to distinguish methodological differences, we retain the overall structure of the analyses of Guo *et al.* [32], Dellar [17], and Hou *et al.* [25]. Our analysis is based on the D2Q9 method.

We choose to develop the scheme of Dellar because, in its original form without a source term (or a body force), it is efficient (due to a careful choice of nonhydrodynamic modes N, J_x, and J_y [17] with zero equilibria), robust, and straightforward to implement.

The MRT LBE with a force term can be expressed in the following form:

$$f_i(\mathbf{x} + \mathbf{c_i}\delta t, t + \delta t) = f_i(\mathbf{x}, t) + \sum_j A_{ij}\big[f_j^{(0)}(\mathbf{x}, t) - f_j(\mathbf{x}, t)\big]$$
$$+ \delta t\, F_i, \qquad (A1)$$

where the equilibrium distribution function $f_j^{(0)}$ is in the form

$$f_j^{(0)} = \rho t_j\big(1 + 3u_\alpha c_{j\alpha} + \tfrac{9}{2}u_\alpha u_\beta c_{j\alpha} c_{j\beta} - \tfrac{3}{2}u_\gamma u_\gamma\big), \quad (A2)$$

and where the source term F_i has the following properties:

$$\sum_i F_i = 0, \quad \sum_i \mathbf{c}_i F_i = n\mathbf{F},$$

$$\sum_i \mathbf{c}_i \mathbf{c}_i F_i = \frac{1}{2}[\mathbf{C} + \mathbf{C}^T], \quad (A3)$$

where n is a scalar to be determined, and $\mathbf{C}$ is a function of $\mathbf{F}$ to be determined. Dellar's [17] eigenvalues and corresponding left-row eigenvectors for the collision matrix A_{ij} can be tabulated as in Table I, where we define

$$P_{\alpha\beta} \equiv \Pi^{(0)}_{\alpha\beta} + \Pi^{(1)}_{\alpha\beta} \quad (A4)$$

for $\alpha, \beta \in [x, y]$, and the $\Pi^{(p)}_{\alpha\beta}$ have the usual meaning (see later).

The equilibria are considered in more detail later. From Table I, matrix A_{ij} has the following properties, which, it will be seen, are necessary if one is to recover correct hydrodynamics:

$$\sum_i 1_i A_{ij} = 0, \quad (A5)$$

$$\sum_i c_{i\alpha} A_{ij} = 0, \quad (A6)$$

$$\sum_i c_{i\alpha} c_{i\beta} A_{ij} = \lambda_3 c_{j\alpha} c_{j\beta}. \quad (A7)$$

Here α and β represent either the x or y direction in the lattice grid. We also assume that the lattice basis $\mathbf{c}_i$ and the corresponding weights t_i have the following symmetry properties:

$$\sum_i t_i = 1, \quad (A8)$$

$$\sum_i t_i (c_{i\alpha})^{2p+1} = 0, \quad p \geqslant 0, \quad (A9)$$

$$\sum_i t_i c_{i\alpha} c_{i\beta} = \frac{1}{3} \delta_{\alpha\beta}, \quad (A10)$$

$$\sum_i t_i c_{i\alpha} c_{i\beta} c_{i\gamma} c_{i\theta} = \frac{1}{9}(\delta_{\alpha\beta}\delta_{\gamma\theta} + \delta_{\alpha\gamma}\delta_{\beta\theta} + \delta_{\alpha\theta}\delta_{\beta\gamma}), \quad (A11)$$

where $\delta_{\alpha\beta}$ is the Kronecker delta such that $\delta_{\alpha\beta} = 1$ for $\alpha = \beta$ and 0 otherwise. The weighting t_i is effectively the same as found in Hou *et al.* [25], i.e., $t_0 = \frac{4}{9}$, $t_{\text{odd}} = \frac{1}{36}$, and $t_{\text{even}} = \frac{1}{9}$. See Fig. 5 for the definition of our link vectors and indexing.
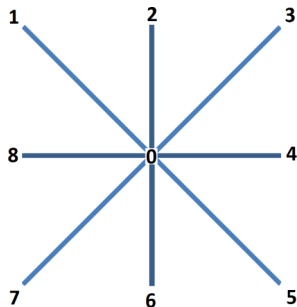

FIG. 5. Schematic of a square lattice in D2Q9 with the indexing convention used throughout.

Note that the six left-row eigenvectors $\mathbf{h}^{(0)} \cdots \mathbf{h}^{(6)}$ that appear in Eqs. (A5)–(A7), as defined in Table I, are linearly independent but not orthogonal. We will return to this matter later. We follow Benzi *et al.* [15,16] and Dellar [17] in selecting the other three "ghost" eigenvectors (see Table I), for which it is important to note the following choice:

$$g_0 = 1, \quad g_{\text{odd}} = 4, \quad g_{\text{even}} = -2. \quad (A12)$$

Next, we conduct an analysis of the LBE method in MRT with a force term, and we compare our results with the single-relaxation-time (SRT) case of Guo *et al.* [32]. The Chapman-Enskog expansion method is used to expand the distribution function around the equilibrium and to reflect the changes in different time scales as follows:

$$f_i = f_i^{(0)} + \epsilon f_i^{(1)} + \epsilon^2 f_i^{(2)} + \cdots, \quad (A13)$$

$$\frac{\partial}{\partial t} = \frac{\partial}{\partial t_0} + \epsilon \frac{\partial}{\partial t_1} + \epsilon^2 \frac{\partial}{\partial t_2} \cdots. \quad (A14)$$

The expansion parameter ϵ can be interpreted as the Knudsen number, which is proportional to the ratio of the lattice spacing to the characteristic flow length. Conservation laws after the expansion still apply as $\sum_i f_i^{(0)} = \rho$ and $\sum_i f_i^{(0)} \mathbf{c}_i = \rho\mathbf{u}$. As the equilibrium distribution accounts for the entire density and momentum locally, this means $\sum_i f_i^{(p)} = 0$ and $\sum_i f_i^{(p+1)} \mathbf{c}_i = 0$ for $p \geqslant 1$, but it is important to note that

$$\rho\mathbf{u} = \sum_i f_i \mathbf{c}_i + m\mathbf{F}\delta t \Leftrightarrow \sum_i f_i^{(1)} \mathbf{c}_i = -m\mathbf{F}\delta t, \quad (A15)$$

where m is a constant to be determined.

Equation (9b) of [32] Guo *et al.* can be rewritten as the following in MRT:

$$O(\epsilon): \quad (c_{i\alpha}\partial_\alpha + \partial_{t_0}) f_i^{(0)} = -\frac{1}{\delta t} \sum_j A_{ij} f_j^{(1)} + F_i. \quad (A16)$$

Taking summation $\sum_i$ on both sides of Eq. (A16) leads to

$$\partial_\alpha \sum_i f_i^{(0)} c_{i\alpha} + \partial_{t_0} \sum_i f_i^{(0)} = -\frac{1}{\delta t} \sum_{ij} A_{ij} f_j^{(1)} + \sum_i F_i = 0. \quad (A17)$$

Using property (A5), we therefore obtain

$$\partial_\alpha \rho u_\alpha + \partial_{t_0} \rho = 0, \quad (A18)$$

which gives the continuity equation and is the MRT equivalent of Eq. (10a) in [32].

Multiplying every term of Eq. (A16) by c_{ix} and taking summation $\sum_i$ on both sides, we have

$$O(\epsilon): \sum_i (c_{i\alpha}\partial_\alpha + \partial_{t_0}) f_i^{(0)} c_{ix}$$

$$= -\frac{1}{\delta t} \sum_{ij} c_{ix} A_{ij} f_j^{(1)} + \sum_i F_i c_{ix}, \quad (A19)$$

where $\sum_i F_i c_{ix} = nF_x$, n is a constant to be determined, and we will use property (A6). As in [25], the momentum flux tensor is defined as $\Pi^{(p)}_{\alpha\beta} = \sum_i f_i^{(p)} c_{i\alpha} c_{i\beta}$. Equation (A22) can

be simplified to produce the Euler equation:

$$\partial_\alpha \Pi^{(0)}_{\alpha x} + \partial_{t_0} \rho u_x = n F_x, \qquad (A20)$$

where the zeroth-order momentum flux tensor $\Pi^{(0)}_{\alpha x} = c_s^2 \rho \delta_{\alpha x} + \rho u_\alpha u_x$, and $\delta_{\alpha x}$ is the Kronecker delta. Equation (A20) is the MRT equivalence of (10b) in [32]. We note that the equivalent result in Guo *et al.* [32] couples n, m, and τ (the collision parameter) in the case of the SRT variant. Following Guo *et al.* [32], we recover the appropriate form of the Euler equation by setting

$$n = 1, \qquad (A21)$$

with no constraint on m at $O(\epsilon)$.

Proceeding to $O(\epsilon)^2$, Eq. (9c) of [32] can be rewritten as the following in MRT:

$$O(\epsilon^2): \partial_{t_1} f_i^{(0)} + (c_{i\alpha}\partial_\alpha + \partial_{t_0}) f_i^{(1)}$$
$$- \frac{1}{2}(c_{i\alpha}\partial_\alpha + \partial_{t_0}) \sum_j A_{ij} f_j^{(1)}$$
$$= -\frac{1}{2}(c_{i\alpha}\partial_\alpha + \partial_{t_0})\delta t F_i. \qquad (A22)$$

Taking summation $\sum_i$ on both sides of Eq. (A22) and simplifying the equation gives

$$\partial_{t_1}\rho = \left(m - \frac{n}{2}\right)\delta t \partial_\alpha F_\alpha. \qquad (A23)$$

This is equivalent to (13a) of [32] in MRT. We recover appropriate dynamics by requiring

$$m - \frac{n}{2} = 0 \Leftrightarrow m = \frac{1}{2}. \qquad (A24)$$

A similar treatment can be performed on Eq. (A22) by multiplying every term by c_{iy} and taking summation $\sum_i$ on both sides:

$$O(\epsilon^2): \partial_{t_1}\sum_i f_i^{(0)} c_{iy} + \partial_\alpha \sum_i f_i^{(1)} c_{i\alpha} c_{iy} + \partial_{t_0}\sum_i f_i^{(1)} c_{iy}$$
$$- \frac{1}{2}\partial_\alpha \sum_{ij} c_{i\alpha} c_{iy} A_{ij} f_j^{(1)} - \frac{1}{2}\partial_{t_0}\sum_{ij} c_{ij} A_{ij} f_j^{(1)}$$
$$= -\frac{1}{2}\delta t \partial_\alpha \sum_i c_{i\alpha} c_{iy} F_i - \frac{1}{2}\delta t \partial_{t_0}\sum_i c_{iy} F_i, \qquad (A25)$$

where the second-order moment of F_i, $\sum_i c_{i\alpha} c_{iy} F_i$, can be calculated as $\frac{1}{2}(C_{\alpha y} + C_{y\alpha})$ according to Guo *et al.* in [32]. Using property (A7), Eq. (A25) can be simplified as

$$\partial_{t_1}(\rho u_y) = \delta t \left(m - \frac{n}{2}\right)\partial_{t_0} F_y + \partial_\alpha \sigma'_{\alpha y}, \qquad (A26)$$

where the viscous stress tensor $\sigma'_{\alpha y}$ is given by

$$\sigma'_{\alpha y} = -\left(1 - \frac{\lambda_3}{2}\right)\Pi^{(1)}_{\alpha y} - \frac{\delta t}{4}(C_{\alpha y} + C_{y\alpha}), \qquad (A27)$$

and where $\Pi^{(1)}_{\alpha\beta}$ represents the first-order momentum flux. In Eq. (A26), the first term on the right-hand side is eliminated by our previous choice of $n = 1$, $m = \frac{1}{2}$. Equation (A26) is the MRT equivalent of Eq. (13b) in [32]. The assignment of $m = \frac{1}{2}$ agrees with Guo *et al.*, but we note that the constraint

imposed by these authors ($n + \frac{m}{\tau} = 1$) does not arise in our analysis. This has consequences later.

The viscous stress defined above ensures that the $O(\epsilon^2)$ dynamics defined in (A26) has a form that can recover the overall Navier-Stokes dynamics, as we now show. Let us first use Eq. (A7) to transform

$$\Pi^{(1)}_{\alpha y} \equiv \sum_j f_j^{(1)} c_{j\alpha} c_{jy} = \frac{1}{\lambda_3}\sum_{ij} c_{i\alpha} c_{iy} A_{ij} f_j^{(1)}. \quad (A28)$$

Then Eq. (A26) may be written as

$$\partial_{t_1}(\rho u_y) + \left(1 - \frac{\lambda_3}{2}\right)\partial_\alpha \left(\frac{1}{\lambda_3}\sum_{ij} c_{i\alpha} c_{iy} A_{ij} f_j^{(1)}\right)$$
$$+ \frac{1}{4}\delta t \partial_\alpha (C_{y\alpha} + C_{\alpha y}) = 0. \qquad (A29)$$

Choosing an appropriate form for **C** (see below) and using the symmetry properties of the lattice, the product rule, and $O(\epsilon)$ dynamics, we obtain, after lengthy algebra,

$$\partial_{t_1}(\rho u_y) - \frac{1}{3}\left(\frac{1}{\lambda_3} - \frac{1}{2}\right)\delta t \partial_\alpha (\rho \partial_\alpha u_y + \rho \partial_y u_\alpha) = 0. \quad (A30)$$

It is important to note that to obtain Eq. (A30), we follow Guo *et al.* [32] and set

$$C_{\alpha\beta} = \left(1 - \frac{\lambda_3}{2}\right)(u_\alpha F_\beta + u_\beta F_\alpha). \qquad (A31)$$

Combining Eqs. (A30) and (A20), we obtain the Navier-Stokes equation for a fluid subject to a body force F:

$$\partial_t \rho u_\alpha + \partial_\beta \rho u_\alpha u_\beta = -\partial_\alpha p + \nu \partial_\beta (\rho \partial_\alpha u_\beta + \rho \partial_\beta u_\alpha) + F_\alpha, \qquad (A32)$$

where the pressure $p = c_s^2 \rho = \frac{1}{3}\rho$ and the kinematic viscosity $\nu = \frac{1}{6}(\frac{2}{\lambda_3} - 1)\delta t$. The source term F_i in Eq. (A1) is given by

$$F_i = t_p \left[3\mathbf{F}\cdot\mathbf{c}_i + \frac{9}{2}\left(1 - \frac{\lambda_3}{2}\right)(F_\alpha u_\beta + F_\beta u_\alpha)\right.$$
$$\left. \times \left(c_{i\alpha}c_{i\beta} - \frac{1}{3}\delta_{\alpha\beta}\right)\right]. \qquad (A33)$$

The above source term is broadly similar to that derived by Guo *et al.* for the LBGK scheme, with eigenvalue λ_3 replacing $\frac{1}{\tau}$. However, there are unexpected differences. Compared with Eq. (20) in Guo *et al.* [32], we note that there is no velocity correction to the first term in Eq. (A33), nor does the factor $(1 - \frac{\lambda_3}{2})$ attach to that term. This is a consequence of raising Guo's constraint $n + \frac{m}{\tau} = 1$, as indicated above.

Let us consider the encapsulation of the collision source term above within the evolution of the modes defined in Table I. In doing so, the advantages of Dellar's original MRT scheme (without a source term) will be seen to be preserved, and we shall be able to produce a collision algorithm that is particularly efficient and implementable.

Define a matrix of left-row eigenvectors:

$$\mathbf{M} \equiv (\mathbf{h}^{(0)}, \mathbf{h}^{(1)}, \ldots, \mathbf{h}^{(8)})^T, \qquad (A34)$$

so that

$$\mathbf{M}\mathbf{f} = (\rho, \rho u_x, \rho u_y, \sigma_{xx}, \sigma_{yy}, \sigma_{xy}, N, J_x, J_y)^T. \quad (A35)$$

The evolution equation (A1) may be projected over the modes, $\mathbf{h^{(n)}}$, defined in Table I, using multiplication by $\mathbf{M}$ from the left:

$$\mathbf{M} \mathbf{f}^+ = \mathbf{M} \mathbf{f} + \mathbf{M} \mathbf{A} \mathbf{M}^{-1}(\mathbf{M} \mathbf{f}^{(0)} - \mathbf{M} \mathbf{f}) + \mathbf{M} \mathbf{F}, \quad \text{(A36)}$$

where $\mathbf{F}$ denotes the column vector with elements F_i, and vectors $\mathbf{f}$, $\mathbf{f}^+$, and $\mathbf{f}^{(0)}$ are regarded as column vectors. Recall that the preceding CE expansion has already assumed that the $\mathbf{h^{(n)}}$ are left (row) eigenvectors of $\mathbf{A}$, that is,

$$\mathbf{M} \mathbf{A} = \Lambda \mathbf{M} \Leftrightarrow \Lambda = \mathbf{M} \mathbf{A} \mathbf{M}^{-1}, \quad \text{(A37)}$$

with Λ a diagonal matrix:

$$\Lambda = \text{diag}(\lambda_0, \lambda_1, \ldots, \lambda_8), \quad \text{(A38)}$$

where $\lambda_0 = \lambda_1 = \lambda_2 = 0$, $\lambda_3 = \lambda_4 = \lambda_5$, and $\lambda_7 = \lambda_8$. We shall return to this point shortly. Clearly, therefore, Eq. (A36) may be written

$$\mathbf{h}^+ = \mathbf{h} + \Lambda(\mathbf{h}^{(0)} - \mathbf{h}) + \mathbf{M} \mathbf{F}, \quad \text{(A39)}$$

or in component form:

$$h^{(p)+} = h^{(p)} + \lambda_p(h^{(0)(p)} - h^{(p)}) + S^{(p)}, \quad p \in [0, Q], \text{(A40)}$$

where the projection of the source term F_i in the evolution equation (A1) gives a "modal" source:

$$S^{(p)} = \sum_{j=0}^{8} M_{pj} F_j. \quad \text{(A41)}$$

We aim to determine the modal source terms $S^{(p)}$, then to invert the transformation in Eq. (A36) above. Bearing in mind the structure of $\mathbf{M}$, it is straightforward using Guo *et al.*'s results to show that

$$S^{(0)} = (\mathbf{h}^{(0)} \circ \mathbf{F}) = \sum_i h_i^{(0)} F_i = A \equiv 0, \quad \text{(A42)}$$

$$S^{(1)} = (\mathbf{h}^{(1)} \circ \mathbf{F}) = \sum_i h_i^{(1)} F_i = \sum_i c_{ix} F_i = nF_x \delta_t, \quad \text{(A43)}$$

$$S^{(2)} = (\mathbf{h}^{(2)} \circ \mathbf{F}) = \sum_i h_i^{(2)} F_i = \sum_i c_{iy} F_i = nF_y \delta_t, \quad \text{(A44)}$$

$$S^{(3)} = (\mathbf{h}^{(3)} \circ \mathbf{F}) = \sum_i h_i^{(3)} F_i = \sum_i c_{ix}^2 F_i = \frac{1}{2}(C_{xx} + C_{xx}), \quad \text{(A45)}$$

$$S^{(4)} = (\mathbf{h}^{(4)} \circ \mathbf{F}) = \sum_i h_i^{(4)} F_i = \sum_i c_{iy}^2 F_i = \frac{1}{2}(C_{yy} + C_{yy}), \quad \text{(A46)}$$

$$S^{(5)} = (\mathbf{h}^{(5)} \circ \mathbf{F}) = \sum_i h_i^{(5)} F_i = \sum_i c_{ix} c_{iy} F_i = \frac{1}{2}(C_{xy} + C_{yx}), \quad \text{(A47)}$$

$$S^{(6)} = (\mathbf{h}^{(6)} \circ \mathbf{F}) = \sum_i h_i^{(6)} F_i = \sum_i g_i F_i = 0, \quad \text{(A48)}$$

$$S^{(7)} = (\mathbf{h}^{(7)} \circ \mathbf{F}) = \sum_i h_i^{(7)} F_i = \sum_i g_i c_{ix} F_i = 0, \quad \text{(A49)}$$

$$S^{(8)} = (\mathbf{h}^{(8)} \circ \mathbf{F}) = \sum_i h_i^{(8)} F_i = \sum_i g_i c_{iy} F_i = 0. \quad \text{(A50)}$$

We note that the source term F_i has no projection onto the nonhydrodynamic modes N, J_x, and J_y. The modal projections of the equilibria are also required:

$$(\mathbf{h}^{(0)} \circ \mathbf{f}^{(0)}) = \sum_i h_i^{(0)} f_i^{(0)} = \sum_i 1_i f_i^{(0)} = \rho, \quad \text{(A51)}$$

$$(\mathbf{h}^{(1)} \circ \mathbf{f}^{(0)}) = \sum_i h_i^{(1)} f_i^{(0)} = \sum_i c_{ix} f_i^{(0)} = \rho u_x, \quad \text{(A52)}$$

$$(\mathbf{h}^{(2)} \circ \mathbf{f}^{(0)}) = \sum_i h_i^{(2)} f_i^{(0)} = \sum_i c_{iy} f_i^{(0)} = \rho u_y, \quad \text{(A53)}$$

$$(\mathbf{h}^{(3)} \circ \mathbf{f}^{(0)}) = \sum_i h_i^{(3)} f_i^{(0)} = \sum_i c_{ix}^2 f_i^{(0)} = \Pi_{xx}^{(0)}, \quad \text{(A54)}$$

$$(\mathbf{h}^{(4)} \circ \mathbf{f}^{(0)}) = \sum_i h_i^{(4)} f_i^{(0)} = \sum_i c_{iy}^2 f_i^{(0)} = \Pi_{yy}^{(0)}, \quad \text{(A55)}$$

$$(\mathbf{h}^{(5)} \circ \mathbf{f}^{(0)}) = \sum_i h_i^{(5)} f_i^{(0)} = \sum_i c_{ix} c_{iy} f_i^{(0)} = \Pi_{xy}^{(0)}, \quad \text{(A56)}$$

$$(\mathbf{h}^{(6)} \circ \mathbf{f}^{(0)}) = \sum_i h_i^{(6)} f_i^{(0)} = \sum_i g_i f_i^{(0)} = 0, \quad \text{(A57)}$$

$$(\mathbf{h}^{(7)} \circ \mathbf{f}^{(0)}) = \sum_i h_i^{(7)} f_i^{(0)} = \sum_i g_i c_{ix} f_i^{(0)} = 0, \quad \text{(A58)}$$

$$(\mathbf{h}^{(8)} \circ \mathbf{f}^{(0)}) = \sum_i h_i^{(8)} f_i^{(0)} = \sum_i g_i c_{iy} f_i^{(0)} = 0. \quad \text{(A59)}$$

We now find from Eq. (A40) and Table I the following "forced" modal evolution equations:

$$i = 0 : \rho^+ = \rho, \quad \text{(A60)}$$

$$i = 1 : (\rho u_x)^+ = \rho u_x + nF_x \delta_t, \quad \text{(A61)}$$

$$i = 2 : (\rho u_y)^+ = \rho u_y + nF_y \delta_t, \quad \text{(A62)}$$

$$i = 3 \cdots 5 : (P_{\alpha\beta})^+ = P_{\alpha\beta} - \lambda_3 (P_{\alpha\beta} - \Pi_{\alpha\beta}^{(0)}) + \frac{\delta t}{2}(C_{\alpha\beta} + C_{\beta\alpha}), \quad \text{(A63)}$$

$$i = 6 : N^+ = N - \lambda_6 N, \quad \text{(A64)}$$

$$i = 7,8 : J_\alpha^+ = J_\alpha - \lambda_7 J_\alpha, \quad \text{(A65)}$$

where $\alpha, \beta \in [x, y]$. We note the simple form of the relaxation equations for $\mathbf{h}^{(6)}, \ldots, \mathbf{h}^{(8)}$, i.e., N, J_x, J_y, which for $\lambda_6 = \lambda_7 = 1$ reduce to $N^+ = J_x^+ = J_y^+ = 0$. This is a direct consequence of the choice of equilibria.

Let us define column vectors $\mathbf{k}^{(n)}$ for $n = 0, \ldots, 8$ as follows:

$$k_i^{(0)} = 2t_i - \frac{3}{2}t_i(c_{ix}^2 + c_{iy}^2), \quad \text{(A66)}$$

$$k_i^{(1)} = 3t_i c_{ix}, \quad \text{(A67)}$$

$$k_i^{(2)} = 3t_i c_{iy}, \quad \text{(A68)}$$

$$k_i^{(3)} = \frac{9}{2}t_i c_{ix}^2 - \frac{3}{2}t_i, \quad \text{(A69)}$$

$$k_i^{(4)} = \frac{9}{2}t_i c_{iy}^2 - \frac{3}{2}t_i, \quad \text{(A70)}$$

$$k_i^{(5)} = 9t_i c_{ix} c_{iy}, \quad \text{(A71)}$$

$$k_i^{(6)} = \tfrac{1}{4} g_i t_i, \tag{A72}$$

$$k_i^{(7)} = \tfrac{3}{8} g_i t_i c_{ix}, \tag{A73}$$

$$k_i^{(8)} = \tfrac{3}{8} g_i t_i c_{iy}. \tag{A74}$$

It is straightforward using lattice properties (A8)–(A11) to show that $\mathbf{k}^{(n)}$ has the property

$$(\mathbf{h}^{(i)} \circ \mathbf{k}^{(j)}) = \delta_{ij}. \tag{A75}$$

Hence it is immediate that

$$\mathbf{M}^{-1} = (\mathbf{k}^{(0)}, \mathbf{k}^{(1)}, \dots, \mathbf{k}^{(8)}). \tag{A76}$$

Having found $\mathbf{M}^{-1}$, it is now possible to reconstruct a postcollision distribution function vector $\mathbf{f}^+$:

$$\mathbf{f}^+ = \mathbf{M}^{-1}\,\mathbf{h}^+, \tag{A77}$$

which, along with Eq. (A40), gives

$$
\begin{aligned}
f_i^+ &= (M)_{ij}^{-1} h_j^+ \\
&= t_i \Big\{ \big[2 - \tfrac{3}{2}\big(c_{ix}^2 + c_{iy}^2\big) \big]\rho + 3[(\rho u_x)^+ c_{ix} + (\rho u_y)^+ c_{iy}] \\
&\quad + \tfrac{9}{2}\big(P_{xx}^+ c_{ix}^2 + 2 P_{xy}^+ c_{ix} c_{iy} + P_{yy}^+ c_{iy}^2 \big) - \tfrac{3}{2}(P_{xx}^+ + P_{yy}^+) \\
&\quad + \tfrac{1}{4} g_i N^+ + \tfrac{3}{8} g_i (J_x^+ c_{ix} + J_y^+ c_{iy}) \Big\}, \tag{A78}
\end{aligned}
$$

with the $(\rho u_x)^+$, $(\rho u_y)^+$, ρ^+, P_{xx}^+, P_{xy}^+, P_{yy}^+, N^+, J_x^+, and J_y^+ determined in Eqs. (A60)–(A65).

APPENDIX B: STRUCTURE OF THE MATRIX A

From Eq. (A37), we have

$$\mathbf{A} = \mathbf{M}\,\Lambda\,\mathbf{M}^{-1}, \tag{B1}$$

with Λ, $\mathbf{M}$, and $\mathbf{M}^{-1}$ given in Eqs. (A38), (A34), and (A76), respectively. The **A** matrix has the following form:

$$
\mathbf{A} = \frac{\lambda_3}{12}
\begin{bmatrix}
0 & -16 & -8 & -16 & -8 & -16 & -8 & -16 & -8 \\
0 & 5 & 1 & -1 & 1 & 5 & 1 & -1 & 1 \\
0 & 2 & 4 & 2 & -2 & 2 & 4 & 2 & -2 \\
0 & -1 & 1 & 5 & 1 & -1 & 1 & 5 & 1 \\
0 & 2 & -2 & 2 & 4 & 2 & -2 & 2 & 4 \\
0 & 5 & 1 & -1 & 1 & 5 & 1 & -1 & 1 \\
0 & 2 & 4 & 2 & -2 & 2 & 4 & 2 & -2 \\
0 & -1 & 1 & 5 & 1 & -1 & 1 & 5 & 1 \\
0 & 2 & -2 & 2 & 4 & 2 & -2 & 2 & 4
\end{bmatrix}
$$

$$
+ \frac{\lambda_6}{36}
\begin{bmatrix}
4 & 16 & -8 & 16 & -8 & 16 & -8 & 16 & -8 \\
1 & 4 & -2 & 4 & -2 & 4 & -2 & 4 & -2 \\
-2 & -8 & 4 & -8 & 4 & -8 & 4 & -8 & 4 \\
1 & 4 & -2 & 4 & -2 & 4 & -2 & 4 & -2 \\
-2 & -8 & 4 & -8 & 4 & -8 & 4 & -8 & 4 \\
1 & 4 & -2 & 4 & -2 & 4 & -2 & 4 & -2 \\
-2 & -8 & 4 & -8 & 4 & -8 & 4 & -8 & 4 \\
1 & 4 & -2 & 4 & -2 & 4 & -2 & 4 & -2 \\
-2 & -8 & 4 & -8 & 4 & -8 & 4 & -8 & 4
\end{bmatrix}
$$

$$
+ \frac{\lambda_7}{12}
\begin{bmatrix}
0 & 0 & 0 & 0 & 0 & 0 & 0 & 0 & 0 \\
0 & 4 & -1 & 0 & 1 & -4 & 1 & 0 & -1 \\
0 & -4 & 2 & -4 & 0 & 4 & -2 & 4 & 0 \\
0 & 0 & -1 & 4 & -1 & 0 & 1 & -4 & 1 \\
0 & 4 & 0 & -4 & 2 & -4 & 0 & 4 & -2 \\
0 & -4 & 1 & 0 & -1 & 4 & -1 & 0 & 1 \\
0 & 4 & -2 & 4 & 0 & -4 & 2 & -4 & 0 \\
0 & 0 & 1 & -4 & 1 & 0 & -1 & 4 & -1 \\
0 & -4 & 0 & 4 & -2 & 4 & 0 & -4 & 2
\end{bmatrix}. \tag{B2}
$$

The collision matrix in Eq. (B2) has a form that does not respect the structure one might expect in a physical symmetry argument. Bearing in mind the lattice symmetries apparent in Fig. 5, we would expect the matrix **A** to have the structure presented in Fig. 6.

In Fig. 6, we assume a number of symmetry constraints, for example the scattering between directions 2 and 4, and 2 and 6 is in the same ratio as that between 1 and 3 and 1 and 5. The notation $\mathbf{a}(\Delta\theta, rsf)$ represents elements of **A**, where $\Delta\theta$ indicates the angle between the coupled lattice links in degrees, and r, s, and f denote rest, slow speed, and fast speed links, respectively.

Initial inspection indicates 15 degrees of freedom (DOFs), and we proceed without assuming $a_{ij} = a_{ji}$ (DOF reduces to 9 if we assume $a_{ij} = a_{ji}$). Note that λ_6 alone determines important coupling between rest and moving links:

$$a(-, rr) = \frac{4}{36}\lambda_6, \quad a(-, fr) = \frac{1}{36}\lambda_6, \quad a(-, sr) = \frac{-2}{36}\lambda_6, \tag{B3}$$

which effectively imposes a constraint upon the microscopic dynamics:

$$a(-, rr) = 4a(-, fr) = -2a(-, sr). \tag{B4}$$

We can seek physical constraints further to reduce the number of DOFs. One "obvious" choice is to regularize the scattering on the fast and slow sublattices:

$$\frac{a(180, ss)}{a(180, ff)} = \frac{a(90, ss)}{a(90, ff)} = \frac{a(-, rs)}{a(-, rf)} \equiv k, \tag{B5}$$

where $k \in \mathbb{R}$ leads to three equations in matrix form:

$$
\begin{bmatrix}
12 - 15k & 4(1-k) & -6(1-2k) \\
3(-2+k) & 4(1-k) & 0 \\
-24(1-2k) & -8(1+2k) & 0
\end{bmatrix}
\begin{bmatrix}
\lambda_3 \\
\lambda_6 \\
\lambda_7
\end{bmatrix} = \mathbf{0}. \tag{B6}
$$

	0	1	2	3	4	5	6	7	8
0	a(-, rr)	a(-, rf)	a(-, rs)	a(-, rf)	a(-, rs)	a(-, rf)	a(-, rs)	a(-, rf)	a(-, rs)
1	a(-, fr)	a(0, ff)	a(45, fs)	a(90, ff)	a(135, fs)	a(180, ff)	a(135, fs)	a(90, ff)	a(45, fs)
2	a(-, sr)	a(45, sf)	a(0, ss)	a(45, sf)	a(90, ss)	a(135, sf)	a(180, ss)	a(135, sf)	a(90, ss)
3	a(-, fr)	a(90, ff)	a(45, fs)	a(0, ff)	a(45, fs)	a(90, ff)	a(135, fs)	a(180, ff)	a(135, fs)
4	a(-, sr)	a(135, sf)	a(90, ss)	a(45, sf)	a(0, ss)	a(45, sf)	a(90, ss)	a(135, sf)	a(180, ss)
5	a(-, fr)	a(180, ff)	a(135, fs)	a(90, ff)	a(45, fs)	a(0, ff)	a(45, fs)	a(90, ff)	a(135, fs)
6	a(-, sr)	a(135, sf)	a(180, ss)	a(135, sf)	a(90, ss)	a(45, sf)	a(0, ss)	a(45, sf)	a(90, ss)
7	a(-, fr)	a(90, ff)	a(135, fs)	a(180, ff)	a(135, fs)	a(90, ff)	a(45, fs)	a(0, ff)	a(45, fs)
8	a(-, sr)	a(45, sf)	a(90, ss)	a(135, sf)	a(180, ss)	a(135, sf)	a(90, ss)	a(45, sf)	a(0, ss)

FIG. 6. Structure of matrix **A** subject to lattice symmetries.

The above equations have a nontrivial solution if the determinant of the matrix vanishes, which leads to

$$k = \frac{1}{2} \in \mathbb{R}, \, k = \frac{3 \pm \sqrt{7}i}{4} \in \mathbb{C}. \quad (B7)$$

Unfortunately, $k = \frac{1}{2}$ results in $\lambda_3 = \lambda_6 = 0$.

If we relax our requirement to

$$\frac{a(90,ss)}{a(90,ff)} = \frac{a(-,rs)}{a(-,rf)} = k, \quad (B8)$$

the submatrix structure apparent in Eq. (B6) again does not allow a physical solution. The most illuminating analysis may be to apply Gaussian elimination in the system (B6) to obtain eigenvalue relations:

$$\lambda_7 = \frac{3(1-k)}{1-2k}\lambda_3, \quad (B9)$$

$$\lambda_6 = \frac{3(2-k)}{4(1-k)}\lambda_3, \quad (B10)$$

where λ_3 will be chosen to set the lattice fluid viscosity. By respecting the above conditions, therefore, some of the physical structure of **A** will be embedded. In general, however, it is clear that the problem is overspecified.

APPENDIX C: A MODIFIED EXPRESSION FOR AVERAGE EMULSION STRESS

We consider, for simplicity, a sheared emulsion of solid spheres at low concentration, in a liquid with shear viscosity η_0. We follow Landau and Lifshitz [19], modifying their analysis slightly to allow for that body force density within the liquid necessary within the lattice Boltzmann equation simulation. We will easily find the necessary correction term.

The mean value, over volume, of the momentum flux Π_{ik} is, in the linear approximation with respect to velocity, the same as the mean of the stress, i.e., $\overline{\sigma_{ik}} = \frac{1}{V} \int \sigma_{ik} dV$, which is identical to

$$\overline{\sigma_{ik}} = \eta_0 \left(\frac{\overline{\partial v_i}}{\partial x_k} + \frac{\overline{\partial v_k}}{\partial x_i} \right) - \overline{p}\delta_{ik}$$

$$+ \frac{1}{V} \int \left[\sigma_{ik} - \eta_0 \left(\frac{\partial v_i}{\partial x_k} + \frac{\partial v_k}{\partial x_i} \right) + p\delta_{ik} \right] dV. \quad (C1)$$

To evaluate the volume integral in the above, it is convenient to use the divergence theorem [19], which may be accomplished by transforming the stress using the identity $\sigma_{ik} = \frac{\partial}{\partial x_l}(\sigma_{il}x_k)$. This result relies upon Stokes' equation $\frac{\partial \sigma_{il}}{\partial x_l} = 0$. Now, Stokes' equation must be modified in the presence of a body force density, **F**, to read $\frac{\partial \sigma_{il}}{\partial x_l} = -F_i$, whereupon we must revise the necessary identity:

$$\sigma_{ik} = \frac{\partial}{\partial x_l}(\sigma_{il}x_k) + x_k F_i. \quad (C2)$$

Substituting this result into Eq. (C1), we are easily able to recover Eq. (22.6) of Landau and Lifshitz [19] for the average transport of momentum in an emulsion (by making identical arguments, of course) but with the addition of a small correction term that should vanish as the resolution employed in the simulations increases:

$$\overline{\sigma_{ik}} = \eta_0 \left(\frac{\overline{\partial v_i}}{\partial x_k} + \frac{\overline{\partial v_k}}{\partial x_i} \right) + 5\eta_0 \alpha_{ik} \frac{4\pi R^3}{3}c - \int x_k F_i dV, \quad (C3)$$

where α_{ik} is the shear rate [19]. Hence, when computing the average stresses within the liquid drop emulsions in Sec. III, in which an immersed boundary, i.e., a body force, acts, it is necessary to correct and to include the following in the computation of the extra term:

$$\delta\sigma_{ik} = -\int x_k F_i dV. \quad (C4)$$

[1] A. K. Gunstensen, D. H. Rothman, S. Zaleski, and G. Zanetti, Phys. Rev. A **43**, 4320 (1991).

[2] M. R. Swift, W. R. Osborn, and J. M. Yeomans, Phys. Rev. Lett. **75**, 830 (1995).

[3] M. R. Swift, E. Orlandini, W. R. Osborn, and J. M. Yeomans, Phys. Rev. E **54**, 5041 (1996).

[4] A. J. Wagner, Phys. Rev. E **74**, 056703 (2006).

[5] Q. Li and A. J. Wagner, Phys. Rev. E **76**, 036701 (2007), and references therein.

[6] A. J. Wagner and C. M. Pooley, Phys. Rev. E **76**, 045702(R) (2007).

[7] X. Shan and H. Chen, Phys. Rev. E **49**, 2941 (1994).

[8] S. V. Lishchuk, C. M. Care, and I. Halliday, Phys. Rev. E **67**, 036701 (2003).

[9] I. Halliday, A. P. Hollis, and C. M. Care, Phys. Rev. E **76**, 026708 (2007).

[10] M. M. Dupin, I. Halliday, and C. M. Care, Phil. Trans. Roy. Soc. A **362**, 1775 (2004).

[11] M. M. Dupin, I. Halliday, and C. M. Care, Med. Eng. Phys. **28**, 13 (2006).

[12] T. J. Spencer, I. Halliday, and C. M. Care, Phys. Rev. E **82**, 066701 (2010).

[13] T. Lee and P. F. Fischer, Phys. Rev. E **74**, 046709 (2006).

[14] C. M. Pooley and K. Furtado, Phys. Rev. E **77**, 046702 (2008).

[15] R. Benzi, S. Succi, and M. Vergassola, Europhys. Lett. **13**, 727 (1990).

[16] R. Benzi, S. Succi, and M. Vergassola, Phys. Rep. **222**, 145 (1992).

[17] P. J. Dellar, Phys. Rev. E **65**, 036309 (2002).

[18] J. Happel and H. Brenner, *Low Reynolds Number Hydrodynamics*, 2nd ed. (Noordhoff International, Leyden, 1973).

[19] L. Landau and E. M. Lifshitz, *Fluid Mechanics*, 6th ed. (Pergamon, London, 1966).

[20] I. Halliday, S. V. Lishchuk, T. J. Spencer, G. Pontrelli, and C. M. Care, Phys. Rev. E **87**, 023307 (2013), and references therein.

[21] U. D'Ortona, D. Salin, M. Cieplak, R. B. Rybka, and J. R. Banavar, Phys. Rev. E **51**, 3718 (1995).

[22] G. I. Taylor, Proc. R. Soc. London, Ser. A **138**, 133 (1932).

[23] A. J. Wagner and I. Pagonabarraga, J. Stat. Phys. **107**, 521 (2002).

[24] E. Lorenz, A. G. Hoekstra, and A. Caiazzo, Phys. Rev. E **79**, 036706 (2009).

[25] S. Hou, Q. Zou, S. Chen, G. Doolen, and A. C. Cogley, J. Comput. Phys. **118**, 329 (1995).

[26] W. Rybczynski, Bull. Acad. Sci. Cracovie (Ser. A) 40 (1911) and also J. S. Hadamard, C. R. Acad. Sci. (Paris) **152**, 1735 (1911); **154**, 109 (1912).

[27] H. Lamb, *Hydrodynamics*, 6th ed. (Cambridge University Press, Cambridge, 1932).

[28] A. Einstein, Ann. Phys. **324**, 289 (1906); and a correction to that article, *ibid.* **339**, 591 (1911).

[29] G. I. Taylor and A. Acrivos, J. Fluid. Mech. **18**, 466 (1964).

[30] J. Boussinesq, Comput. Rend. Acad. Sci. (Paris) **156**, 124 (1913).

[31] Y. H. Qian, D. d'Humières, and P. Lallemand, Europhys. Lett. **17**, 479 (1992).

[32] Z. Guo, C. Zheng, and B. Shi, Phys. Rev. E **65**, 046308 (2002).